Pressure-Induced Double-Dome Superconductivity in Kagome Metals $A\mathrm{Ti_3Bi_5}$ (A = Cs, Rb)

J. Y. Nie(聂嘉颖)[1,2†], X. F. Yang(杨小帆)[3†*], K. Y. Chen(陈凯运)[3†], X. Q. Liu(刘祥麒)[4†], W. Xia(夏威)[4,5], J. Wang(王晶)[1], R. Zhang(张蕊)[3], D. Z. Dai(戴东喆)[1], C. C. Zhao(赵成成)[1], C. P. Tu(涂成鹏)[1], H. L. Dong(董洪亮)[6,7], X. B. Jin(靳小博)[1], J. K. Deng(邓俊楷)[8], X. Zhang(张旭)[1*], Y. F. Guo(郭艳峰)[4,5*], and S. Y. Li(李世燕)[1,2,9,10*]

[1]*State Key Laboratory of Surface Physics, Department of Physics, Fudan University, Shanghai 200438, China*
[2]*Shanghai Research Center for Quantum Sciences, Shanghai 201315, China*
[3]*Northwest Institute for Non-ferrous Metal Research, Xi'an 710016, China*
[4]*School of Physical Science and Technology, ShanghaiTech University, Shanghai 201210, China*
[5]*ShanghaiTech Laboratory for Topological Physics, Shanghai 201210, China*
[6]*Center for High Pressure Science and Technology Advanced Research, Shanghai 201203, China*
[7]*Shanghai Key Laboratory of Material Frontiers Research in Extreme Environments, Institute for Shanghai Advanced Research in Physical Sciences, Shanghai 201203, China*
[8]*State Key Laboratory for Mechanical Behavior of Materials, Xi'an Jiaotong University, Xi'an 710049, China*
[9]*Shanghai Branch, Hefei National Laboratory, Shanghai 201315, China*
[10]*Collaborative Innovation Center of Advanced Microstructures, Nanjing 210093, China*

(Received 14 May 2025; accepted manuscript online 29 May 2025)

The recently discovered titanium-based kagome metal $A\mathrm{Ti_3Bi_5}$ (A = Cs, Rb) provides a new platform to explore novel quantum phenomena. In this work, the transport properties of $A\mathrm{Ti_3Bi_5}$ (A = Cs, Rb) are systematically investigated under high pressure. Although $A\mathrm{Ti_3Bi_5}$ (A = Cs, Rb) shows no evidence of superconductivity at ambient pressure, the pressure-induced double-dome superconductivity is observed in both compounds, resembling the superconducting phase diagram of $A\mathrm{V_3Sb_5}$ (A = Cs, Rb, and K) under pressure. High-pressure X-ray diffraction measurements exclude the pressure-induced structural phase transition. A slope change in the c/a ratio was found between 12.4 and 14.9 GPa, indicating the occurrence of lattice distortion. The distinct changes in the electronic band structure revealed by first-principles calculations further explain the emergence of superconductivity in the two domes. These findings suggest that pressure can effectively tune the electronic properties of $A\mathrm{Ti_3Bi_5}$, providing new insights into the rich physics of kagome metals.

DOI: 10.1088/0256-307X/42/7/070713 CSTR: 32039.14.0256-307X.42.7.070713

The kagome lattice, a two-dimensional network with corner-sharing triangles, stimulates a wide variety of investigations into correlated electronic phenomena and nontrivial topological states.[1] With this special geometry, the kagome lattice naturally possesses unique electronic structures including flat bands, Dirac points, and van Hove singularities (VHSs), which give rise to a series of novel quantum phenomena, such as quantum spin liquid,[2,3] fractional quantum Hall states,[4–6] density waves,[7,8] and unconventional superconductivity.[9–11]

Among kagome materials, the vanadium-based superconductor $A\mathrm{V_3Sb_5}$ (A = Cs, Rb and K) has aroused tremendous interest.[12–14] In $A\mathrm{V_3Sb_5}$, the VHSs at the M point are located close to the Fermi level and induce charge-density-wave (CDW) order with a transition temperature of $T_{\mathrm{CDW}} \sim 78$–103 K.[15–18] However, it still remains unclear whether the CDW order originates from Fermi surface nesting or electron–phonon coupling.[17,19–25] Additionally, $A\mathrm{V_3Sb_5}$ exhibits a superconducting transition with $T_c \sim 0.9$–2.5 K.[12–14,18] Until now, the nature of pairing symmetry is still under hot debate.[26–32] The intertwined superconductivity and charge order display a complicated phase diagram under pressure.[33–44] Despite extensive studies focused on $A\mathrm{V_3Sb_5}$, the underlying mechanism of these novel quantum phenomena remains elusive.[18,45,46]

The titanium-based kagome metal $A\mathrm{Ti_3Bi_5}$ (A = Cs, Rb), which is isostructural with $A\mathrm{V_3Sb_5}$, has been synthesized more recently.[47–49] Non-trivial $\mathbb{Z}_2$ topological band structures, including flat bands, Dirac nodal lines, and possible topological surface states, were revealed by angular-resolved photoemission spectroscopy (ARPES) measurements and density functional theory (DFT) calculations.[50–54] Compared with $A\mathrm{V_3Sb_5}$,

†These authors contributed equally to this work.
*Corresponding authors. Email: yangxiaofan@fudan.edu.cn; xuzhang_fd@fudan.edu.cn; guoyf@shanghaitech.edu.cn; shiyan_li@fudan.edu.cn
© 2025 Chinese Physical Society and IOP Publishing Ltd. All rights, including for text and data mining, AI training, and similar technologies, are reserved.

the phonon dispersion of $A\mathrm{Ti_3Bi_5}$ is free of imaginary frequencies,[53,55] and the VHSs at the M point are pushed far above the Fermi level, in line with the absence of CDW order.[51–53,56] Orbital-selective electronic nematicity was evidenced by angular-dependent magnetoresistance, scanning tunneling microscopy (STM), and polarization-dependent ARPES measurements.[49,54,57] Although signatures of superconductivity in $A\mathrm{Ti_3Bi_5}$ were claimed by Yang *et al.*,[49,54] metallic behavior with no obvious anomaly down to 2 K was reported by other groups.[48,52,56] By carrier doping or applying pressure, the position of these unique electronic structures can be tuned over a large energy range,[50,51,58] which may give rise to some exotic physical properties, such as superconductivity. In this sense, with the absence of the CDW order, $A\mathrm{Ti_3Bi_5}$ serves as a promising reference material to $A\mathrm{V_3Sb_5}$ to understand the novel phenomena and electronic properties in the kagome lattice.

Applying pressure is a clean and effective method to tune the electronic and structural properties of quantum materials without introducing impurities. In this study, we present high-pressure resistance measurements on $A\mathrm{Ti_3Bi_5}$ (A = Cs, Rb) to investigate the evolution of its electronic properties. Despite $A\mathrm{Ti_3Bi_5}$ showing no evidence of superconductivity at ambient pressure, pressure-induced double-dome superconductivity is observed in both compounds. The first superconducting dome of $\mathrm{CsTi_3Bi_5}$ starts at $\sim$2 GPa, accompanied by the appearance of a new Fermi pocket that enhances the density of states near the Fermi level, according to our first-principles calculations. The superconducting transition temperature T_c reaches its first maximum of 1.10 K at $\sim$6 GPa. Then, the superconductivity is gradually suppressed by pressure and disappears at $\sim$13 GPa. However, with further compression, the superconductivity re-emerges with a second maximum of 0.84 K at $\sim$ 15 GPa, then finally vanishes at $\sim$ 36 GPa, showing a typical double-dome phase diagram. The reappearance of superconductivity is accompanied by the pressure-induced lattice distortion and changes in band structure. Similar double-dome superconductivity is also observed in compressed $\mathrm{RbTi_3Bi_5}$. Compared to $\mathrm{CsTi_3Bi_5}$, the two superconducting domes of $\mathrm{RbTi_3Bi_5}$ span a narrower regime in the phase diagram, similar to the situation in $A\mathrm{V_3Sb_5}$. Our results demonstrate that applying pressure can effectively tune the electronic band structure of $A\mathrm{Ti_3Bi_5}$, which may have a significant impact on the interplay between superconducting and nematic order in this novel kagome material.

Single crystals of $A\mathrm{Ti_3Bi_5}$ (A = Cs, Rb) were grown by the self-flux method.[48] Since $A\mathrm{Ti_3Bi_5}$ single crystals are sensitive to air, all samples were prepared under an argon atmosphere to avoid degradation. For each measurement, we used a fresh piece of $A\mathrm{Ti_3Bi_5}$ single crystal and peeled off the surface with Scotch tape to ensure purity. The X-ray diffraction (XRD) measurement was performed using an X-ray diffractometer (D8 Advance, Bruker) with Cu $K\alpha$ radiation (wavelength λ = 1.5418 Å). The resistance and specific heat measurements under ambient pressure were performed using a physical property measurement system (PPMS, Quantum Design), with a very short exposure time to air (several minutes).

High pressure was generated by a diamond anvil cell (DAC) made from Be–Cu alloy. The diamond culet was 400 μm in diameter. A mixture of epoxy and fine cubic boron nitride powder was used to cover the Be–Cu gasket. A 150 μm sample chamber was drilled at the center of the pre-indented pit, in which a piece of $A\mathrm{Ti_3Bi_5}$ single crystal was loaded (under an argon atmosphere) with NaCl powder surrounding it as a pressure transmitting medium. Platinum foils with a thickness of 4 μm were used as electrodes. The pressure inside the DAC was determined by the ruby fluorescence method at room temperature each time before and after the measurement.[59] High-pressure resistance was measured in a ^{3}He cryostat with the van der Pauw method.

High-pressure XRD experiments were performed on a $\mathrm{CsTi_3Bi_5}$ powder sample at room temperature at the BL15U1 beamline of the Shanghai Synchrotron Radiation Facility (wavelength λ = 0.6199 Å). A symmetrical DAC with 300 μm culets was used to generate pressure. A 100 μm sample chamber was drilled from a stainless-steel gasket, and Daphne 7373 oil was used as the pressure transmitting medium. Pressure was also calibrated by the ruby fluorescence method.[59] The XRD images were integrated using the Dioptas software.[60] The diffraction patterns were analyzed with Le Bail refinement by the GSAS-II software.[61]

The first-principles calculations were carried out with DFT implemented in the Vienna *ab initio* simulation package (VASP).[62,63] The exchange-correlation functional was treated by the generalized gradient approximation and parameterized by the Perdew–Burke–Ernzerhof functional.[64] The DFT-D3 method of Grimme with a zero-damping function[65] was adopted to correct the influence from van der Waals interactions and the spin–orbit coupling was taken into account in all the calculations. The plane wave cutoff was set to 550 eV. The Monkhorst-Pack k-point mesh of $13 \times 13 \times 7$ was employed for the unit cell. The convergence tolerance was 10^{-6} eV for total energy and all forces were converged to be $< 0.005\,\mathrm{eV\AA^{-1}}$.

As plotted in Fig. 1(a), $A\mathrm{Ti_3Bi_5}$ shows a layered hexagonal structure ($P6/mmm$, No. 191).[48] The Ti–Bi and A layers are alternately stacked along the c axis. Each Ti–Bi layer contains a kagome net of titanium atoms, with bismuth positioned within the hexagons and both above and below the triangles. The XRD patterns of the largest natural surface for $A\mathrm{Ti_3Bi_5}$ single crystals are shown in Fig. 1(b). Only $(00l)$ Bragg peaks are observed, indicating that it is the ab plane. The lattice constant c is determined to be 9.263 Å for $\mathrm{CsTi_3Bi_5}$ and 9.144 Å for $\mathrm{RbTi_3Bi_5}$, respectively. Typical resistivity curves of $A\mathrm{Ti_3Bi_5}$ at ambient pressure are plotted in Fig. 1(c), showing metallic behavior without a superconducting transition down to 1.8 K. The absence of superconductivity is also verified by the specific heat data, which can be well fitted by $C_\mathrm{p} = \gamma T + AT^3$ with the Sommerfeld coefficient

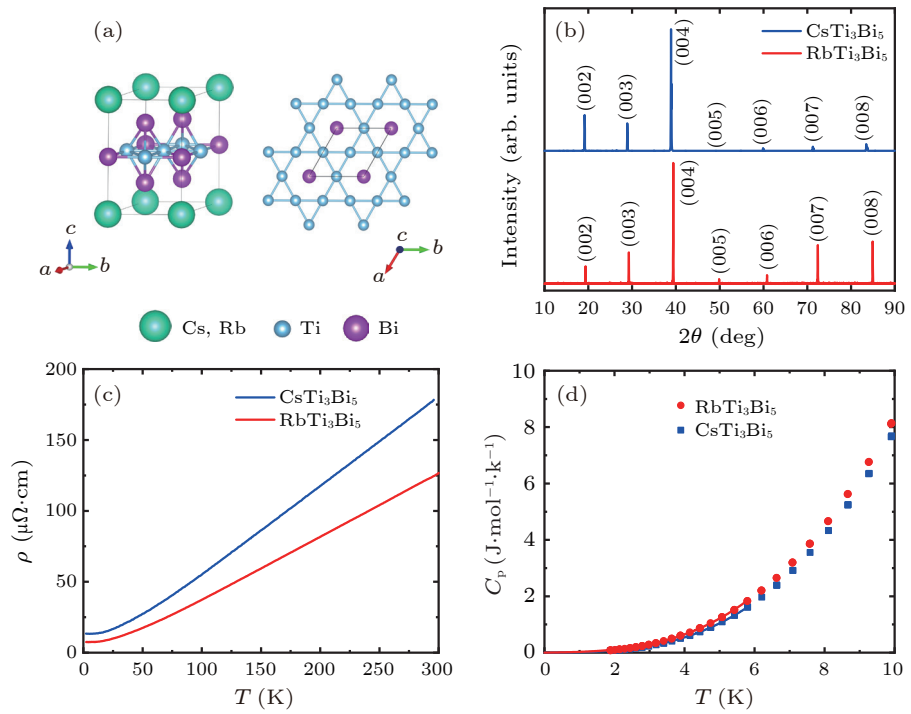

Fig. 1. (a) Side and top views of the crystal structure of ATi_3Bi_5 (A = Cs, Rb). The titanium atoms form a perfect kagome net with bismuth atoms in the hexagons. The A, Ti, and Bi atoms are represented as green, blue, and violet balls. (b) XRD patterns of the largest natural surface for $CsTi_3Bi_5$ (blue curve) and $RbTi_3Bi_5$ (red curve) single crystals. (c) Temperature dependence of resistivity for $CsTi_3Bi_5$ and $RbTi_3Bi_5$ single crystals at ambient pressure. (d) Low-temperature specific heat of $CsTi_3Bi_5$ and $RbTi_3Bi_5$ single crystals. The solid lines show the fitting of the data below 6 K to $C_p = \gamma T + AT^3$.

$\gamma = 6.1\,\mathrm{mJ\cdot mol^{-1}\cdot K^{-2}}$ for $CsTi_3Bi_5$ and $19.2\,\mathrm{mJ\cdot mol^{-1}\cdot K^{-2}}$ for $RbTi_3Bi_5$ [Fig. 1(d)]. However, tiny superconducting transitions with onset temperatures of 4.8 K and 4.2 K are observed in the magnetic susceptibility of $CsTi_3Bi_5$ and $RbTi_3Bi_5$ single crystals, respectively (data not shown). Their superconducting volume fractions are estimated to be less than 0.01% at 2 K under a magnetic field of 10 Oe. It is very likely that the superconducting transitions come from tiny impurities of superconducting $CsBi_2$ ($T_c = 4.65$ K) and $RbBi_2$ ($T_c = 4.21$ K).[66] Therefore, ATi_3Bi_5 (A = Cs, Rb) itself is a nonsuperconducting kagome metal, consistent with previous reports.[48,52,56]

Figures 2(a) and 2(b) present the low-temperature resistance of $CsTi_3Bi_5$ ranging from 0.9 to 36.5 GPa. All the data are normalized at 3 K and vertically shifted for clarity. The transition temperature T_c is defined as the temperature at which the resistance drops to 90% of its normal-state value. At 0.9 GPa, no superconducting transition is observed in $CsTi_3Bi_5$ down to 0.3 K, which further confirms the absence of superconductivity at ambient pressure. By applying pressure, superconductivity emerges, and T_c is gradually enhanced to 1.10 K at 6.2 GPa. As pressure increases, T_c shifts to lower temperatures and cannot be detected at 12.7 GPa, showing the first superconducting dome. Apart from the low-temperature superconducting transitions, no anomalies are observed in the resistance curves up to 10 K, and the observed T_c values differ significantly from those of elemental Bi under pressure,[67] thereby ruling out the possibility that the superconductivity originates from Bi impurity. With further compression, the superconducting transition reappears and T_c increases to a second maximum of 0.84 K at 15.3 GPa. Then T_c decreases again, and the superconducting transition completely vanishes at 36.5 GPa, exhibiting the second superconducting dome.

To confirm the pressure-induced resistance drop is related to a superconducting transition, various magnetic fields were applied on $CsTi_3Bi_5$ at 15.3 GPa, as shown in Fig. 2(c). It can be seen that the resistance drop is monotonically suppressed with increasing magnetic fields and completely vanishes in 0.3 T. This result demonstrates that the resistance drop under pressure is indeed a superconducting transition. The temperature dependence of the upper critical field $\mu_0 H_{c2}$ at 15.3 GPa is summarized in the inset of Fig. 2(c). The data can be well fitted by the empirical Ginzburg–Landau (GL) formula $\mu_0 H_{c2}(T) = \mu_0 H_{c2}(0)[1-(T/T_c)^2]/[1+(T/T_c)^2]$. The $\mu_0 H_{c2}(0)$ is determined to be 0.13 T at 15.3 GPa, much lower than the Pauli paramagnetic limit $\mu_0 H_p(0) = 1.84 T_c \approx 1.55$ T, indicating the absence of Pauli pair breaking.

Similar to $CsTi_3Bi_5$, the normalized low-temperature resistance of $RbTi_3Bi_5$ with different pressures ranging from 1.5 to 37.1 GPa is plotted in Figs. 2(d) and 2(e), which also exhibits double-dome superconductivity. The absence of any anomalies above the superconducting transition excludes the possibility that the observed behavior is influenced by Bi impurity.[67] At 1.5 GPa, no superconducting transition is observed in $RbTi_3Bi_5$ down to 0.3 K.

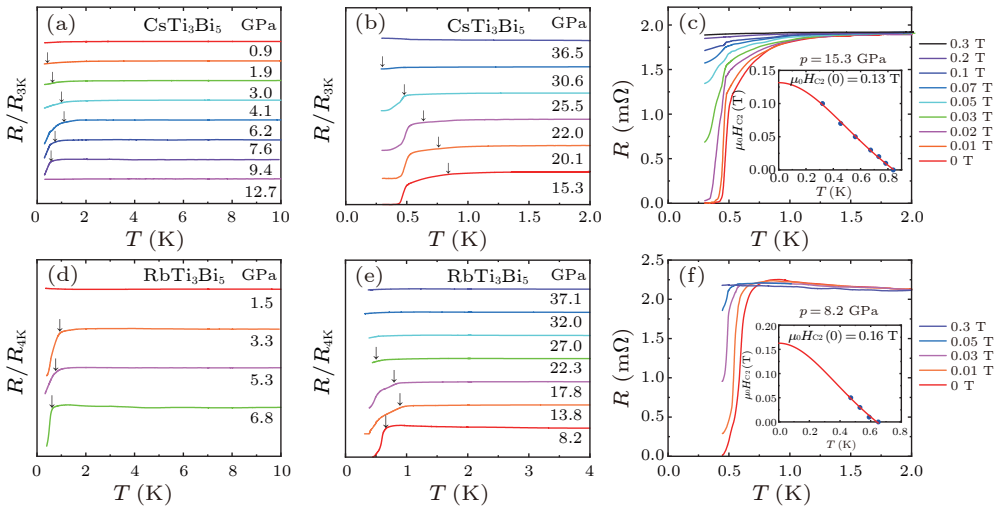

Fig. 2. (a) and (b) Temperature dependence of normalized resistance for $CsTi_3Bi_5$ under various pressures up to 36.5 GPa. (d) and (e) Temperature dependence of normalized resistance for $RbTi_3Bi_5$ under various pressures up to 37.1 GPa. All the data are normalized and vertically shifted for clarity. (c) and (f) Temperature dependence of resistance for $CsTi_3Bi_5$ and $RbTi_3Bi_5$ under different magnetic fields at 15.3 GPa and 8.2 GPa, respectively. The magnetic field gradually suppresses the superconducting transition. The insets show the temperature dependence of the upper critical field $\mu_0 H_{c2}$. The red lines are the fittings of the data to the Ginzburg–Landau formula.

As pressure increases, superconductivity appears and the T_c reaches its first maximum of 0.94 K at 3.3 GPa, then reduces to 0.61 K at 6.8 GPa, showing the first superconducting dome. With further compression, T_c rises to a second maximum of 0.89 K at 13.8 GPa and completely vanishes at 27.0 GPa, revealing the second superconducting dome. The magnetic fields are applied to $RbTi_3Bi_5$ at 8.2 GPa, as shown in Fig. 2(f). The resistance drop is completely suppressed at 0.3 T. The $\mu_0 H_{c2}(T)$ can also be well fitted by the GL formula, giving $\mu_0 H_{c2}(0) = 0.16$ T at 8.2 GPa, which is significantly lower than the Pauli paramagnetic limit $\mu_0 H_p(0) = 1.84 T_c \approx 1.21$ T.

Based on the above high-pressure resistance measurements of ATi_3Bi_5 (A = Cs, Rb), the temperature-pressure (T–p) phase diagram is summarized in Fig. 3. Two superconducting domes can be clearly seen for both compounds, with SC-I under lower pressures and SC-II under higher pressures, similar to the phase diagram of AV_3Sb_5.[38] Compared to $RbTi_3Bi_5$, the superconductivity in $CsTi_3Bi_5$ spans a broader pressure range with a higher maximum T_c, which is consistent with our expectation. Since alkali metals with smaller ionic radii provide additional chemical pressure,[37,39] $RbTi_3Bi_5$ experiences the re-emergence of superconductivity at lower pressures compared to $CsTi_3Bi_5$. Different from the robust superconductivity in CsV_3Sb_5, which persists up to 150 GPa,[37] the superconductivity in $CsTi_3Bi_5$ completely disappears at 36.5 GPa, which may result from the weakened electron–phonon coupling suggested by theoretical calculations.[58]

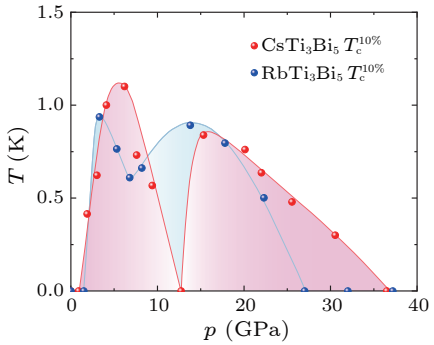

Fig. 3. Temperature-pressure phase diagram of $CsTi_3Bi_5$ and $RbTi_3Bi_5$. Two superconducting domes can be clearly seen for both compounds, with the SC-I phase under lower pressures and the SC-II phase under higher pressures.

To identify the origin of the pressure-induced double-dome superconductivity in $CsTi_3Bi_5$, we performed synchrotron XRD measurements to check the structural stability under high pressure. As depicted in Fig. 4(a), the XRD profile at 1.5 GPa can be well reproduced by space group $P6/mmm$, consistent with the space group at ambient pressure. The black asterisks mark the external signals from different phases of Bi flux, which is unavoidably introduced by the synthesis process.[48] As pressure increases up to 33.1 GPa, all diffraction peaks of $CsTi_3Bi_5$ shift toward higher angles continuously without any evident anomaly, indicating that the crystallographic symmetry is well preserved within the pressure range. Therefore, the re-emergence of superconductivity in $CsTi_3Bi_5$ cannot be attributed to the pressure-induced structural phase transition. The cell volume V, lattice parameters a and c, and c/a ratio are obtained from Le Bail refinement and shown in Figs. 4(b)–4(d). The cell volume gradually reduces with increasing pressures and fits well with the Birch–Murnaghan equation of state,[68] yielding the bulk modulus $B_0 = 58.2$ GPa, its first-order derivative $B_0' = 3.7$ and the zero-pressure volume $V_0 = 262$ Å^3. In comparison with CsV_3Sb_5,[34,37] the bulk modulus of $CsTi_3Bi_5$ is much larger, indicating a stiffer lattice. With increasing pressure, the lattice parameters a and c both decrease. A distinct slope change in the c/a ratio is observed between 12.4 and 14.9 GPa, coinciding with the re-emergence of

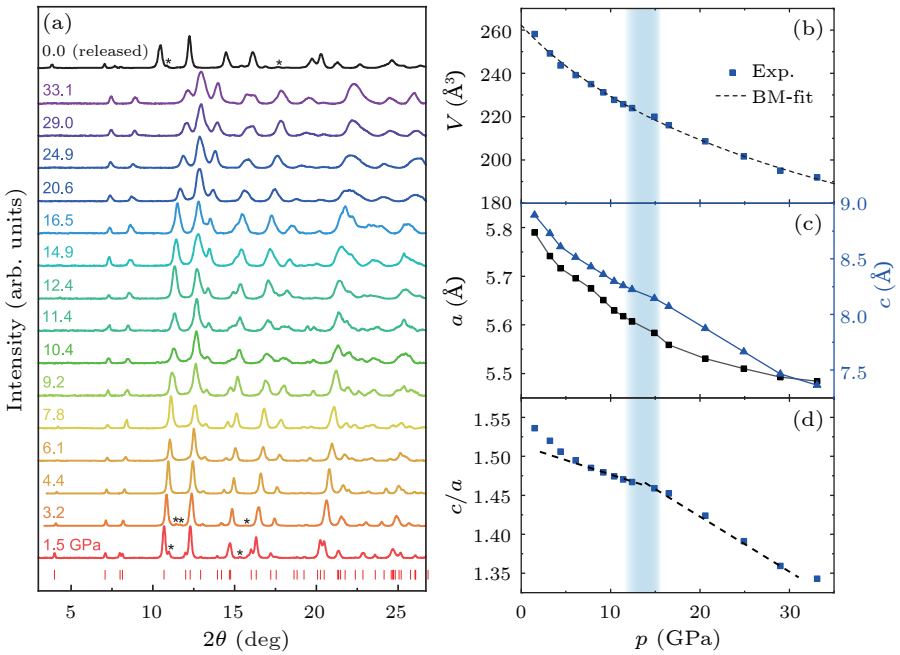

Fig. 4. (a) XRD patterns of $CsTi_3Bi_5$ under high pressure up to 33.1 GPa with an incident wavelength $\lambda = 0.6199$ Å. The patterns for each pressure are normalized to the highest peak intensity after background subtraction. The black asterisks mark the peaks of Bi. (b) The derived cell volume as a function of pressure for $CsTi_3Bi_5$. The black dashed line is a fitting curve by the Birch–Murnaghan equation of state with the derived bulk modulus $B_0 = 58.2$ GPa. (c) Pressure dependence of the lattice parameters a and c for $CsTi_3Bi_5$. (d) Pressure dependence of the c/a ratio for $CsTi_3Bi_5$. The two dashed lines mark the change of slope.

superconductivity. This result suggests that the re-emergent superconductivity may be related to the lattice distortion. It is noteworthy that these pressure-induced lattice changes are reversible, as the diffraction peaks shift back to their initial positions when the pressure is released. This result demonstrates that the kagome lattice of $CsTi_3Bi_5$ is robust in the whole studied pressure range at room temperature, as observed in CsV_3Sb_5.[35]

To reveal the relation between the lattice distortion and the re-emergent superconductivity, we calculate the band structures of $CsTi_3Bi_5$ under various pressures, as shown in Figs. 5(a)–5(d). At 0 GPa, the flat band, two saddle points at the M point and a Dirac point at the K point, which are characterized as the typical features of the kagome lattice, can be clearly seen in Fig. 5(a), consistent with previous reports.[50,58] With increasing pressure, thep orbital of Bi along the Γ–A path gradually shifts upwards. At 1.5 GPa, where the superconducting transition starts to emerge in transport measurements, the p orbital of Bi at the high symmetry point A quickly approaches the Fermi level, creating a small Fermi pocket at the A point and enhancing the density of states near E_F. This distinctive change in the band structure explains the emergence of superconductivity in the SC-I regime. As pressure further increases to 14.9 GPa, where the re-emergent superconductivity in $CsTi_3Bi_5$ reaches its maximum T_c, the VHS related to the minimum point along the Γ–K and Γ–A directions passes by the Fermi level, leading to the second maximum of T_c seen in $CsTi_3Bi_5$. The VHS effectively increases the density of states in the vicinity of the Fermi level, which is beneficial for superconductivity.[69] Therefore, the change in band structure contributes to the emergence of superconductivity in the SC-II phase as well.

The pressure-induced single superconducting dome has been extensively reported in unconventional superconductors.[70–73] In comparison, the presence of two distinct superconducting domes is a relatively uncommon phenomenon. The first superconducting dome is normally associated with the suppression of some ordered phases, arising from quantum fluctuations, while the underlying mechanisms of the second superconducting dome have not been fully understood. Typically, the second dome is accompanied by changes in spin configuration, band structure, or structural phase transition. For instance, in the heavy fermion superconductor $CeCu_2(Si_{1-x}Ge_x)_2$, the low-pressure superconducting dome occurs around the antiferromagnetic quantum critical point, suggesting magnetically mediated pairing, while the high-pressure superconducting dome straddles a weak first-order volume collapse and is believed to be associated with the valence fluctuation of Ce ions.[74–77] In the case of iron chalcogenides $A_xFe_{2-y}Se_2$ [A = K, (Rb, Tl)], after the first maximum T_c of 32 K at 1 GPa, the second superconducting dome then appears above 11.5 GPa with another maximum T_c of 48 K.[78] This is due to the change of Fermi surface topology originating from the structural phase transition.[79] For the vanadium-based kagome superconductor CsV_3Sb_5, the origin of the SC-I phase is strongly related to the CDW instability, and the SC-II phase is attributed to the pressure-induced Lifshitz transition and dimensional crossover.[35,37,40,41,43]

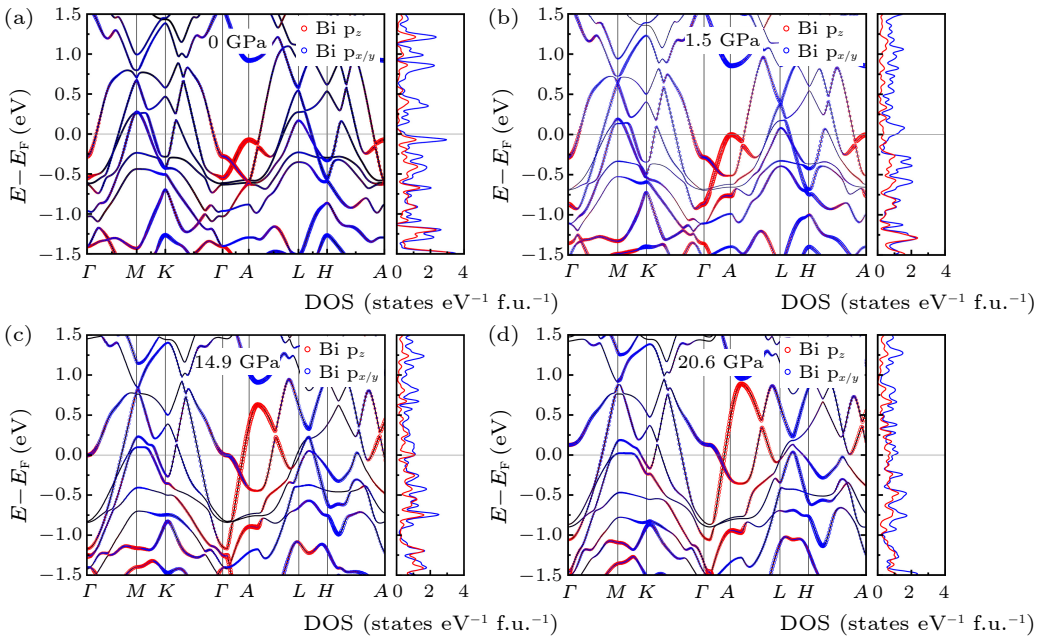

Fig. 5. The projected electronic band structures and partial density of states of Bi $p_{x/y}$ and p_z orbitals of $CsTi_3Bi_5$ at (a) 0, (b) 1.5, (c) 14.9, and (d) 20.6 GPa, respectively.

Unlike CsV_3Sb_5, the SC-I phase of $CsTi_3Bi_5$ does not show CDW order but instead nematic order, identified by the STM measurements.[57] Such intra- and inter-orbital bond nematic orders can arise from the extended Coulomb interaction, which have been studied in connection to the nematic phase of FeSe.[80,81] In this context, the first superconducting dome observed in $CsTi_3Bi_5$ may relate to the instability of the nematic order under pressure. The competition between nematicity and superconductivity may also explain why the theoretically predicted superconductivity is not observed at ambient pressure.[58] Applying pressure hinders the nematicity but changes the band structure, resulting in the emergence of superconductivity. Further investigations, like nuclear magnetic resonance or other experimental techniques, are highly desired to study the nematic phase transition under high pressure.

The double-dome phase diagram and slope change in the c/a ratio of $CsTi_3Bi_5$ are quite similar to that of CsV_3Sb_5, suggesting these two kagome systems may share the same origin of the re-emergent superconductivity. The emergence of the second superconducting dome under high pressure in CsV_3Sb_5 is found to be inherently linked to the interlayer Sb2–Sb2 (Sb atoms that are located out of the kagome plane) interactions.[37] As pressure increases, the distance between Sb2 atoms along the c axis is compressed and c/a exhibits a crossover at T_c minimum.[34,37] The Sb2 atoms form bonds, and the quasi two-dimensional (2D) structure of CsV_3Sb_5 is gradually tuned to a three-dimensional (3D) form.[37] As a result, the p_z orbital of Sb2 gradually passes through the Fermi level, resulting in the enhancement of the density of states and consequently the increase of T_c.[37] Similar to CsV_3Sb_5, pressure effectively changes the interlayer distance in $CsTi_3Bi_5$, leading to a change in the slope of the c/a ratio at T_c minimum. The quasi-2D structure in the isostructural compound $CsTi_3Bi_5$ evolves to a 3D form, and the enhancement of interlayer coupling dramatically tunes the band structure topology of $CsTi_3Bi_5$. The resulting increase in density of states, driven by the VHS at the Γ point near the Fermi level, leads to the emergence of superconductivity in the SC-II regime.

In summary, we investigate the transport properties of kagome metal ATi_3Bi_5 (A = Cs, Rb) under pressures up to 40 GPa. Although ATi_3Bi_5 displays metallic behavior at ambient pressure, superconductivity is induced by pressure, and T_c displays remarkable double domes in the phase diagram. Such double-dome superconductivity under pressure is very similar to that in AV_3Sb_5 (A = Cs, Rb, and K). It is noted that the first superconducting dome accompanies the appearance of a new Fermi pocket, and the second one is related to the change of band structure caused by dimensional crossover under high pressure.

Acknowledgements. This work was supported by the Natural Science Foundation of China (Grant No. 12174064), the Shanghai Municipal Science and Technology Major Project (Grant No. 2019SHZDZX01), and the Innovation Program for Quantum Science and Technology (Grant No. 2024ZD0300104). K.Y.C. acknowledges the support by the Natural Science Foundation of China (Grant No. 12204383), the Young Elite Scientists Sponsorship Program by CAST (Grant No. 2023QNRC001), the Young Talent Fund of the Association for Science and Technology in Shaanxi (Grant No. CLGC202201). Y.F.G. was supported by the open project of Beijing National Laboratory for Condensed Matter Physics (Grant No. ZBJ2106110017) and the Double First-Class Initiative Fund of ShanghaiTech University. The authors thank the staff from BL15U1 at Shanghai Synchrotron Radiation Facility for assistance during data collection.

References

[1] Yin J X, Lian B, and Hasan M Z 2022 *Nature* **612** 647
[2] Norman M R 2016 *Rev. Mod. Phys.* **88** 041002
[3] Yan S, Huse D A, and White S R 2011 *Science* **332** 1173
[4] Tang E, Mei J W, and Wen X G 2011 *Phys. Rev. Lett.* **106** 236802
[5] Neupert T, Santos L, Chamon C, and Mudry C 2011 *Phys. Rev. Lett.* **106** 236804
[6] Bergholtz E J, Liu Z, Trescher M, Moessner R, and Udagawa M 2015 *Phys. Rev. Lett.* **114** 016806
[7] Yu S L and Li J X 2012 *Phys. Rev. B* **85** 144402
[8] Wang W S, Li Z Z, Xiang Y Y, and Wang Q H 2013 *Phys. Rev. B* **87** 115135
[9] Kiesel M L and Thomale R 2012 *Phys. Rev. B* **86** 121105
[10] Kiesel M L, Platt C, and Thomale R 2013 *Phys. Rev. Lett.* **110** 126405
[11] Ko W H, Lee P A, and Wen X G 2009 *Phys. Rev. B* **79** 214502
[12] Ortiz B R, Gomes L C, Morey J R, Winiarski M, Bordelon M, Mangum J S, Oswald I W H, Rodriguez-Rivera J A, Neilson J R, Wilson S D, Ertekin E, McQueen T M, and Toberer E S 2019 *Phys. Rev. Mater.* **3** 094407
[13] Ortiz B R, Teicher S M L, Hu Y, Zuo J L, Sarte P M, Schueller E C, Abeykoon A M M, Krogstad M J, Rosenkranz S, Osborn R, Seshadri R, Balents L, He J, and Wilson S D 2020 *Phys. Rev. Lett.* **125** 247002
[14] Ortiz B R, Sarte P M, Kenney E M, Graf M J, Teicher S M L, Seshadri R, and Wilson S D 2021 *Phys. Rev. Mater.* **5** 034801
[15] Jiang Y X, Yin J X, Denner M M, Shumiya N, Ortiz B R, Xu G, Guguchia Z, He J, Hossain M S, Liu X, Ru J, Kautzsch L, Zhang S S, Chang G, Belopolski I, Zhang Q, Cochran T A, Multer D, Litskevich M, Cheng Z J, Yang X P, Wang Z, Thomale R, Neupert T, Wilson S D, and Hasan M Z 2021 *Nat. Mater.* **20** 1353
[16] Zhao H, Li H, Ortiz B R, Teicher S M L, Park T, Ye M, Wang Z, Balents L, Wilson S D, and Zeljkovic I 2021 *Nature* **599** 216
[17] Tan H, Liu Y, Wang Z, and Yan B 2021 *Phys. Rev. Lett.* **127** 046401
[18] Neupert T, Denner M M, Yin J X, Thomale R, and Hasan M Z 2022 *Nat. Phys.* **18** 137
[19] Zhou X, Li Y, Fan X, Hao J, Dai Y, Wang Z, Yao Y, and Wen H H 2021 *Phys. Rev. B* **104** L041101
[20] Lou R, Fedorov A, Yin Q, Kuibarov A, Tu Z, Gong C, Schwier E F, Büchner B, Lei H, and Borisenko S 2022 *Phys. Rev. Lett.* **128** 036402
[21] Luo H, Gao Q, Liu H, Gu Y, Wu D, Yi C, Jia J, Wu S, Luo X, Xu Y, Zhao L, Wang Q, Mao H, Liu G, Zhu Z, Shi Y, Jiang K, Hu J, Xu Z, and Zhou X J 2022 *Nat. Commun.* **13** 273
[22] Xie Y, Li Y, Bourges P, Ivanov A, Ye Z, Yin J X, Hasan M Z, Luo A, Yao Y, Wang Z, Xu G, and Dai P 2022 *Phys. Rev. B* **105** L140501
[23] Ye Z, Luo A, Yin J X, Hasan M Z, and Xu G 2022 *Phys. Rev. B* **105** 245121
[24] Wenzel M, Ortiz B R, Wilson S D, Dressel M, Tsirlin A A, and Uykur E 2022 *Phys. Rev. B* **105** 245123
[25] Zhu H, Li T, Yu F, Li Y, Wang S, Wu Y, Liu Z, Shang Z, Cui S, Liu Y, Zhang G, Zhang L, Wang Z, Wu T, Ying J, Chen X, and Sun Z 2023 *Chin. Phys. Lett.* **40** 047301
[26] Chen H, Yang H, Hu B, Zhao Z, Yuan J, Xing Y, Qian G, Huang Z, Li G, Ye Y, Ma S, Ni S, Zhang H, Yin Q, Gong C, Tu Z, Lei H, Tan H, Zhou S, Shen C, Dong X, Yan B, Wang Z, and Gao H J 2021 *Nature* **599** 222
[27] Wu X, Schwemmer T, Müller T, Consiglio A, Sangiovanni G, Di Sante D, Iqbal Y, Hanke W, Schnyder A P, Denner M M, Fischer M H, Neupert T, and Thomale R 2021 *Phys. Rev. Lett.* **127** 177001
[28] Xu H S, Yan Y J, Yin R, Xia W, Fang S, Chen Z, Li Y, Yang W, Guo Y, and Feng D L 2021 *Phys. Rev. Lett.* **127** 187004
[29] Zhong Y, Liu J, Wu X, Guguchia Z, Yin J X, Mine A, Li Y, Najafzadeh S, Das D, Mielke III C, Khasanov R, Luetkens H, Suzuki T, Liu K, Han X, Kondo T, Hu J, Shin S, Wang Z, Shi X, Yao Y, and Okazaki K 2023 *Nature* **617** 488
[30] Mu C, Yin Q, Tu Z, Gong C, Lei H, Li Z, and Luo J 2021 *Chin. Phys. Lett.* **38** 077402
[31] Roppongi M, Ishihara K, Tanaka Y, Ogawa K, Okada K, Liu S, Mukasa K, Mizukami Y, Uwatoko Y, Grasset R, Konczykowski M, Ortiz B R, Wilson S D, Hashimoto K, and Shibauchi T 2023 *Nat. Commun.* **14** 667
[32] Zhao C C, Wang L S, Xia W, Yin Q W, Deng H B, Liu G W, Liu J J, Zhang X, Ni J M, Huang Y Y, Tu C P, Tao Z C, Tu Z J, Gong C S, Wang Z W, Lei H C, Guo Y F, Yang X F, Yin J X, and Li S Y 2024 *Chin. Phys. Lett.* **41** 127303
[33] Zhao C C, Wang L S, Xia W, Yin Q W, Ni J M, Huang Y Y, Tu C P, Tao Z C, Tu Z J, Gong C S, Lei H C, Guo Y F, Yang X F, and Li S Y 2021 arXiv:2102.08356
[34] Zhang Z, Chen Z, Zhou Y, Yuan Y, Wang S, Wang J, Yang H, An C, Zhang L, Zhu X, Zhou Y, Chen X, Zhou J, and Yang Z 2021 *Phys. Rev. B* **103** 224513
[35] Chen X, Zhan X, Wang X, Deng J, Liu X B, Chen X, Guo J G, and Chen X 2021 *Chin. Phys. Lett.* **38** 057402
[36] Du F, Luo S, Ortiz B R, Chen Y, Duan W, Zhang D, Lu X, Wilson S D, Song Y, and Yuan H 2021 *Phys. Rev. B* **103** L220504
[37] Yu F, Zhu X, Wen X, Gui Z, Li Z, Han Y, Wu T, Wang Z, Xiang Z, Qiao Z, Ying J, and Chen X 2022 *Phys. Rev. Lett.* **128** 077001
[38] Zhu C C, Yang X F, Xia W, Yin Q W, Wang L S, Zhao C C, Dai D Z, Tu C P, Song B Q, Tao Z C, Tu Z J, Gong C S, Lei H C, Guo Y F, and Li S Y 2022 *Phys. Rev. B* **105** 094507
[39] Du F, Li R, Luo S, Gong Y, Li Y, Jiang S, Ortiz B R, Liu Y, Xu X, Wilson S D, Cao C, Song Y, and Yuan H 2022 *Phys. Rev. B* **106** 024516
[40] Yu F H, Ma D H, Zhuo W Z, Liu S Q, Wen X K, Lei B, Ying J J, and Chen X H 2021 *Nat. Commun.* **12** 3645
[41] Chen K Y, Wang N N, Yin Q W, Gu Y H, Jiang K, Tu Z J, Gong C S, Uwatoko Y, Sun J P, Lei H C, Hu J P, and Cheng J G 2021 *Phys. Rev. Lett.* **126** 247001
[42] Wang N N, Chen K Y, Yin Q W, Ma Y N N, Pan B Y, Yang X, Ji X Y, Wu S L, Shan P F, Xu S X, Tu Z J, Gong C S, Liu G T, Li G, Uwatoko Y, Dong X L, Lei H C, Sun J P, and Cheng J G 2021 *Phys. Rev. Res.* **3** 043018
[43] Zheng L, Wu Z, Yang Y, Nie L, Shan M, Sun K, Song D, Yu F, Li J, Zhao D, Li S, Kang B, Zhou Y, Liu K, Xiang Z, Ying J, Wang Z, Wu T, and Chen X 2022 *Nature* **611** 682
[44] Lin Y P and Nandkishore R M 2022 *Phys. Rev. B* **106** L060507
[45] Jiang K, Wu T, Yin J X, Wang Z, Hasan M Z, Wilson S D, Chen X, and Hu J 2023 *Natl. Sci. Rev.* **10** nwac199
[46] Wilson S D and Ortiz B R 2024 *Nat. Rev. Mater.* **9** 420
[47] Yang H, Zhao Z, Yi X W, Liu J, You J Y, Zhang Y, Guo H, Lin X, Shen C, Chen H, Dong X, Su G, and Gao H J 2022 arXiv:2209.03840
[48] Werhahn D, Ortiz B R, Hay A K, Wilson S D, Seshadri R, and Johrendt D 2022 *Z. Naturforsch. B* **77** 757
[49] Yang H, Ye Y, Zhao Z, Liu J, Yi X W, Zhang Y, Xiao H, Shi J, You J Y, Huang Z, Wang B, Wang J, Guo H, Lin X, Shen C, Zhou W, Chen H, Dong X, Su G, Wang Z, and Gao H J 2024 *Nat. Commun.* **15** 9626

[50] Yang J, Yi X, Zhao Z, Xie Y, Miao T, Luo H, Chen H, Liang B, Zhu W, Ye Y, You J Y, Gu B, Zhang S, Zhang F, Yang F, Wang Z, Peng Q, Mao H, Liu G, Xu Z, Chen H, Yang H, Su G, Gao H, Zhao L, and Zhou X J 2023 *Nat. Commun.* **14** 4089

[51] Liu B, Kuang M Q, Luo Y, Li Y, Hu C, Liu J, Xiao Q, Zheng X, Huai L, Peng S, Wei Z, Shen J, Wang B, Miao Y, Sun X, Ou Z, Cui S, Sun Z, Hashimoto M, Lu D, Jozwiak C, Bostwick A, Rotenberg E, Moreschini L, Lanzara A, Wang Y, Peng Y, Yao Y, Wang Z, and He J 2023 *Phys. Rev. Lett.* **131** 026701

[52] Wang Y, Liu Y, Hao Z, Cheng W, Deng J, Wang Y, Gu Y, Ma X M, Rong H, Zhang F, Guo S, Zhang C, Jiang Z, Yang Y, Liu W, Jiang Q, Liu Z, Ye M, Shen D, Liu Y, Cui S, Wang L, Liu C, Lin J, Liu Y, Cai Y, Zhu J, Chen C, and Mei J W 2023 *Chin. Phys. Lett.* **40** 037102

[53] Jiang Z, Liu Z, Ma H, Xia W, Liu Z, Liu J, Cho S, Yang Y, Ding J, Liu J, Huang Z, Qiao Y, Shen J, Jing W, Liu X, Liu J, Guo Y, and Shen D 2023 *Nat. Commun.* **14** 4892

[54] Hu Y, Le C, Zhang Y, Zhao Z, Liu J, Ma J, Plumb N C, Radovic M, Chen H, Schnyder A P, Wu X, Dong X, Hu J, Yang H, Gao H J, and Shi M 2023 *Nat. Phys.* **19** 1827

[55] Yi X W, Ma X Y, Zhang Z, Liao Z W, You J Y, and Su G 2022 *Phys. Rev. B* **106** L220505

[56] Chen X, Liu X, Xia W, Mi X, Zhong L, Yang K, Zhang L, Gan Y, Liu Y, Wang G, Wang A, Chai Y, Shen J, Yang X, Guo Y, and He M 2023 *Phys. Rev. B* **107** 174510

[57] Li H, Cheng S, Ortiz B R, Tan H, Werhahn D, Zeng K, Johrendt D, Yan B, Wang Z, Wilson S D, and Zeljkovic I 2023 *Nat. Phys.* **19** 1591

[58] Yi X W, Liao Z W, You J Y, Gu B, and Su G 2023 *Research* **6** 0238

[59] Mao H K, Xu J, and Bell P M 1986 *J. Geophys. Res.: Solid Earth* **91** 4673

[60] Prescher C and Prakapenka V B 2015 *High Press. Res.* **35** 223

[61] Toby B H and Von Dreele R B 2013 *J. Appl. Crystallogr.* **46** 544

[62] Kresse G and Furthmüller J 1996 *Phys. Rev. B* **54** 11169

[63] Monkhorst H J and Pack J D 1976 *Phys. Rev. B* **13** 5188

[64] Perdew J P, Burke K, and Ernzerhof M 1996 *Phys. Rev. Lett.* **77** 3865

[65] Grimme S, Antony J, Ehrlich S, and Krieg H 2010 *J. Chem. Phys.* **132** 154104

[66] Gutowska S, Wiendlocha B, Klimczuk T, and Winiarski M J 2023 *J. Phys. Chem. C* **127** 14402

[67] Li Y, Wang E, Zhu X, and Wen H 2017 *Phys. Rev. B* **95** 024510

[68] Birch F 1947 *Phys. Rev.* **71** 809

[69] Luo Y, Han Y, Liu J, Chen H, Huang Z, Huai L, Li H, Wang B, Shen J, Ding S, Li Z, Peng S, Wei Z, Miao Y, Sun X, Ou Z, Xiang Z, Hashimoto M, Lu D, Yao Y, Yang H, Chen X, Gao H J, Qiao Z, Wang Z, and He J 2023 *Nat. Commun.* **14** 3819

[70] Norman M R 2011 *Science* **332** 196

[71] Kusmartseva A F, Sipos B, Berger H, Forró L, and Tutiš E 2009 *Phys. Rev. Lett.* **103** 236401

[72] Cheng J G, Matsubayashi K, Wu W, Sun J P, Lin F K, Luo J L, and Uwatoko Y 2015 *Phys. Rev. Lett.* **114** 117001

[73] Sun J P, Matsuura K, Ye G Z, Mizukami Y, Shimozawa M, Matsubayashi K, Yamashita M, Watashige T, Kasahara S, Matsuda Y, Yan J Q, Sales B C, Uwatoko Y, Cheng J G, and Shibauchi T 2016 *Nat. Commun.* **7** 12146

[74] Yuan H Q, Grosche F M, Deppe M, Geibel C, Sparn G, and Steglich F 2003 *Science* **302** 2104

[75] Yuan H Q, Grosche F M, Deppe M, Sparn G, Geibel C, and Steglich F 2006 *Phys. Rev. Lett.* **96** 047008

[76] Stockert O, Arndt J, Faulhaber E, Geibel C, Jeevan H S, Kirchner S, Loewenhaupt M, Schmalzl K, Schmidt W, Si Q, and Steglich F 2011 *Nat. Phys.* **7** 119

[77] Holmes A T, Jaccard D, and Miyake K 2004 *Phys. Rev. B* **69** 024508

[78] Sun L, Chen X J, Guo J, Gao P, Huang Q Z, Wang H, Fang M, Chen X, Chen G, Wu Q, Zhang C, Gu D, Dong X, Wang L, Yang K, Li A, Dai X, Mao H K, and Zhao Z 2012 *Nature* **483** 67

[79] Yamamoto Y, Yamaoka H, Tanaka M, Okazaki H, Ozaki T, Takano Y, Lin J F, Fujita H, Kagayama T, Shimizu K, Hiraoka N, Ishii H, Liao Y F, Tsuei K D, and Mizuki J 2016 *Sci. Rep.* **6** 30946

[80] Jiang K, Hu J, Ding H, and Wang Z 2016 *Phys. Rev. B* **93** 115138

[81] Zhang P, Qian T, Richard P, Wang X P, Miao H, Lv B Q, Fu B B, Wolf T, Meingast C, Wu X X, Wang Z Q, Hu J P, and Ding H 2015 *Phys. Rev. B* **91** 214503